Wireless Capsule Endoscope for Targeted Drug Delivery: Mechanics and Design Considerations

Stephen P. Woods* and Timothy G. Constandinou, *Senior Member, IEEE*

***Abstract*—This paper describes a platform to achieve targeted drug delivery in the next-generation wireless capsule endoscopy. The platform consists of two highly novel subsystems: one is a micropositioning mechanism which can deliver 1 ml of targeted medication and the other is a holding mechanism, which gives the functionality of resisting peristalsis. The micropositioning mechanism allows a needle to be positioned within a 22.5° segment of a cylindrical capsule and be extendible by up to 1.5 mm outside the capsule body. The mechanism achieves both these functions using only a single micromotor and occupying a total volume of just 200 mm^3. The holding mechanism can be deployed diametrically opposite the needle in 1.8 s and occupies a volume of just 270 mm^3. An in-depth analysis of the mechanics is presented and an overview of the requirements necessary to realize a total system integration is discussed. It is envisaged that the targeted drug delivery platform will empower a new breed of capsule microrobots for therapy in addition to diagnostics for pathologies such as ulcerative colitis and small intestinal Crohn's disease.**

***Index Terms*—Gastrointestinal (GI) tract, microrobot, pill robot, targeted therapy, wireless capsule endoscopy.**

I. Introduction

THERE are a number of wireless capsule endoscopes (WCE) available for detecting and diagnosing pathologies of the gastrointestinal (GI) tract such as small intestinal Crohn's disease, obscure gastrointestinal bleeding (OGIB), and small intestinal tumors.

One such capsule is the M2A developed by Given Imaging Ltd. [1] in 2000. This system was developed specifically for examining the small intestines as conventional endoscopes cannot reach the total length of the GI tract [2]. Its small size of 11.0 mm in diameter × 25.0 mm long allows it to pass through the GI tract under natural peristalsis pressure. Another similar system is the EndoCapsule by Olympus [3]. These systems use onboard CMOS- or CCD-based image sensors to take pictures of the intestinal wall. The pictures can be transmitted to a device worn by the patient for later evaluation. A detailed review of WCE is reported in [4].

Current WCE systems in general do not have the functionality or the onboard capacity to treat pathologies of the GI tract, such as ulcerative colitis, with medication as they are limited to diagnostic use. However, there is a clinical need to target and treat these pathologies [5]; hence, endeavors have been made by researchers such as Philips Electronics with IntelliCap [6], Innovative Devices LLC with the InteliSite [7], and Phaeton Research with the Enterion capsule [8] to perform regional drug absorption services. These systems are capable of delivering up to 1 ml of medication to a region of the GI tract such as the jejunum, ileum, ascending colon, or descending colon either through the progressive release of medication over a period of time or through a bolus form.

The delivery methods employed by these devices prevent the direct targeting of specific pathogens such as tumors or ulcers as the medication is spread over a section of lumen due to the constant movement from peristalsis; further, they have no means of stopping and holding their position.

This paper presents a platform for delivering a targeted dose of medication in a confined compliant tubular environment. The platform comprises a holding mechanism and a needle positioning mechanism, which are integrated into a WCE. This integration gives increased functionality allowing the WCE to be used for targeted drug delivery in the GI tract. Specifically, this paper focuses on the two key mechanisms and is organized as follows: Section II introduces the concept and requirements, Section III describes the holding mechanism for resisting peristalsis, Section IV describes the targeting/delivery mechanism, Section V discusses additional platform considerations required to complete a system realization, and Section VI concludes this study.

II. Concept and Design Requirements

Conventional WCE have sufficiently small geometry to allow them to pass through the small intestines and navigate the ileocolic valve without becoming an obstruction. However, the clinical need to target a specific location or feature within the GI tract for medication delivery or examination of the intestinal wall would require the WCE to stop. Fig. 1 shows a microrobot concept design capable of resisting peristaltic pressure through the deployment of an integrated holding mechanism and targeted drug delivery through the activation of a needle. The needle has the ability to be positioned in a 360° envelope. Simultaneously, the holding mechanism can stay diametrically opposite the needle guaranteeing penetration of the GI tract wall.

Manuscript received June 15, 2012; revised September 13, 2012; accepted October 27, 2012. Date of publication November 21, 2012; date of current version March 15, 2013. This work was supported in part by Duckworth and Kent Ltd. *Asterisk indicates corresponding author.*

*S. P. Woods is with the Department of Electrical and Electronic Engineering and Centre for Bio-Inspired Technology, Institute of Biomedical Engineering, Imperial College London, London SW7 2AZ, U.K., and also with Duckworth & Kent Ltd., Herts. SG7 6XL, U.K. (e-mail: s.woods09@imperial.ac.uk).

T. G. Constandinou is with the Department of Electrical and Electronic Engineering and Centre for Bio-Inspired Technology, Institute of Biomedical Engineering, Imperial College London, London SW7 2AZ, U.K. (e-mail: t.constandinou@imperial.ac.uk).

Color versions of one or more of the figures in this paper are available online at http://ieeexplore.ieee.org.

Digital Object Identifier 10.1109/TBME.2012.2228647

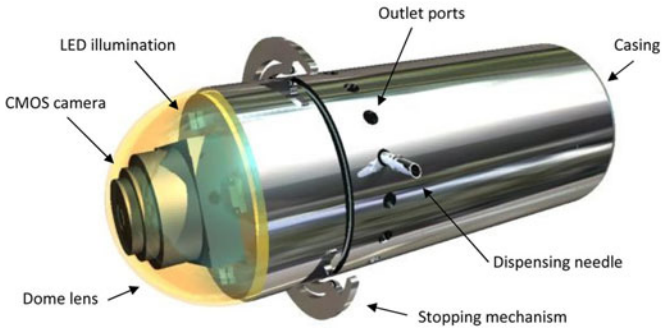

Fig. 1. Microrobot concept design capable of resisting peristaltic pressure through an integrated holding mechanism and delivering 1 ml targeted medication. Holding mechanism shown partially open and the needle fully extended to 1.5 mm outside the capsule body.

A. Movement Analysis of the GI Tract

Once swallowed, the WCE will pass through the elementary canal. The particular section of interest for diagnosis and treatment is the small intestines as this section is very difficult to access. The small intestines comprise of the duodenum, the jejunum, and the ileum. These three sections make up the longest part of the alimentary canal at 6.25 m [9]. The duodenum is C-shaped and its mouth, the ileocolic valve, extends from the stomach giving this section a degree of stability. The jejunum and the ileum are free to move; however, their natural state is collapsed.

In order to process foodstuff, a liquid mixture called chyme, the small intestines use a series of movement patterns. These patterns, segmentation, and peristalsis [10] cause the chyme to progress through the tract. Segmentation is a contraction of the duodenum for the purpose of mixing food. There are two processes involved: they are eccentric contractions and concentric contraction. The first generates very little intraluminal pressure and the second can generate pressures as high as 20 mmHg [10]. The frequency of the contractions is dependent on eating patterns, becoming stronger as chyme is being processed. Peristalsis is the process of moving chyme through the intestinal tract from the stomach to the colon by means of a series of muscle contractions acting in a wave pattern. The muscle contraction acts in two planes: circumferential and longitudinal. Miftahof [11] has developed a mathematical model to describe the dynamics of the electromechanical wave phenomenon of a segment of the gut. They report that the active force of contraction in the longitudinal direction should have an amplitude of 26.9 g/cm and an amplitude of 17.2 g/cm in the circumferential direction. For a conventional WCE with dimensions of 11.0 mm diameter $\times$ 25.0 mm long, the circumferential and longitudinal amplitudes translate into 421.8 and 911.9 mN, respectively. These estimated forces have been used as a guide in the design analysis of the holding mechanism.

B. Resisting Peristalsis and Geometrical Constraints

There are three methods employed for halting the progress of a WCE by enabling it to resist the natural movement from peristalsis. One utilizes microactuator mechanisms embedded within the capsule, such as the paddling-based microrobot developed by Park *et al*. [12]. The second approach exploits external magnetic fields to control the position of the capsule, and the third approach applies a stimulus to GI tract to inhibit peristalsis [13].

There has been much development in the field of magnetic control of WCE such as the magnetic shell employed by Carpi *et al*. [14]. This system looks to modify existing WCE with the addition of a magnetic shell. The shell can be used to guide the WCE by means of an external magnetic field; however, this system requires large equipment to perform the procedure and there is also an increase in the diameter of the WCE.

To overcome peristalsis, a holding mechanism compact enough to fit within the microrobot yet leaves sufficient space for medication and other features are required. There have been a number of systems employed by researchers to stop the microrobot, such as insufflation of the tract using balloons or expanding legs [15]. However, these systems exhibit limitations. In the case of the expanding legs, they are driven by a leadscrew, which is powered by a micromotor. The leadscrew and the micromotor are axially aligned with the microrobot. This configuration requires a substantial amount of space and presents problems of force translation through the legs due to the lever effect.

TABLE I
OVERALL TECHNICAL REQUIREMENTS

Requirement	Specification
Micro-robot volume	maximum 3.0 cm^3
Sensing	pH, temp and pressure
Vision	CMOS and optical dome
Illumination	4 white LEDs
Power source	onboard battery
Tracking	RF and time
Telemetry	bidirectional
Attaining equilibrium	holding
Delivering therapy	liquid medication
Drug reservoir	1 ml

C. Target Technical Specifications

The overall geometry of the microrobotic system will be greatly influenced by the limitations imposed by swallowing and on its ability to navigate natural obstacles such as the ileocolic valve without becoming an obstruction. A patient's ability to swallow a required volume will vary from person to person; therefore, a standard volume must be chosen which will be suitable for the majority of patients. Research carried out by Connor *et al*. shows that a volume of 3.0 cm^3 can be swallowed [16]. This maximum target volume will be required to house all the components necessary to perform targeted therapy and microscale diagnosis. Table I lists the overall technical requirements for the microrobot platform.

D. System Operation Overview

The main sequence of events required to perform a procedure to deliver targeted therapy to the GI tract can be seen in Fig. 2. The procedure starts with the patient ingesting the WCE. Once

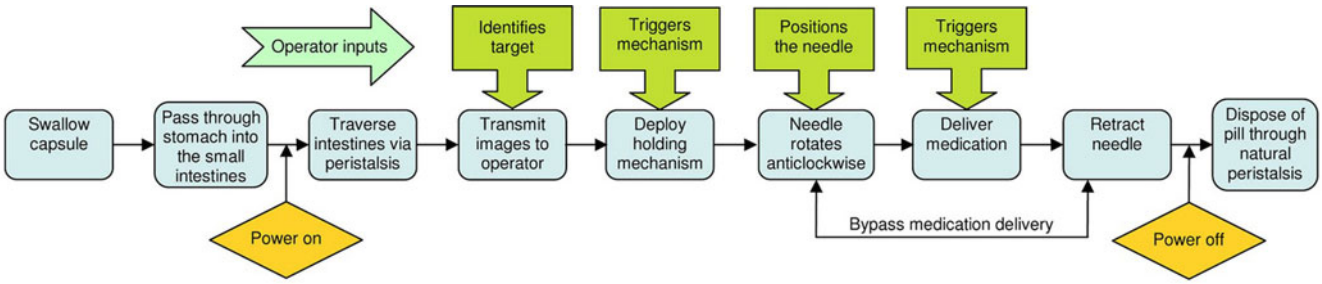

Fig. 2. Flow diagram showing the key stages of operation for a procedure to deliver targeted therapy to the GI tract using a remotely operated WCE.

Fig. 3. (a) Holding mechanism concept which utilizes a vertically orientated micromotor to give the WCE the ability to overcome peristalsis and (b) 3-D internal view of the gear train.

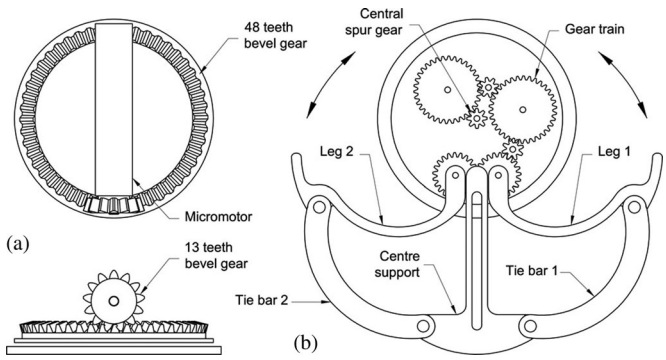

Fig. 4. Holding mechanism design showing: (a) 13 teeth and 48 teeth bevel gears set and (b) gear train and legs in the fully extended position. The central spur gear is driven by the 48 teeth bevel gear.

the capsule passes through the stomach and enters the small intestines, it can begin to transmit images to the operator via an RF link. The real-time images and sensor data will be displayed on an external PC. The operator will use the data to identify an already defined target site. Once the target site has been reached, the operator will remotely deploy the holding mechanism. The operator can now rotate the needle into any one of 16 predefined positions; the position will be based on observational data received just before the deployment of the holding mechanism. The needle can now be advanced into the GI tract wall and the medication released. The targeting mechanism is designed such that it gives the operator the ability to reposition the needle before the medication is delivered. Finally, the capsule will be dispelled through natural peristalsis movement.

III. Holding Mechanism

The holding mechanism in Fig. 3(a) uses a single micromotor to open and close two legs. The two legs are connected to a central support via two pinned leg ties. The two-legged design utilizes a micromotor, which is orientated in a vertical position [see Fig. 4(a)]. The micromotor is connected to a bevel gear set, which allows the micromotor's rotation to be translated through 90°. The bevel gear drives a gear train of spur gears which drive the legs in and out [see Figs. 3(b) and 4(b)]. This novel configuration reduces the micromotor's revolution per minute (RPM). The reduction in RPM will result in a multiplication of the micromotor's torque; this will give the legs the strength required to distend the GI tract wall and hold the microrobot in place.

To secure the microrobot in place, the holding mechanism will be required to expand to a size which is sufficiently large that it resists the natural movement from peristalsis. This is achieved through an increase in circumference of the microrobot. The holding mechanism begins with a circumference of 34.5 mm; however, when activated the mechanism increases in size to produce a circumference of 60.4 mm, which is an increase of 75%. This can be further increased to 71.25 mm by simply modifying the profile of the legs to increase the surface area in contact with the GI tract wall.

The method by which the legs open and close poses the potential risk of tissue becoming trapped in the mechanism; however, the orientation of the legs combined with their smooth rounded ends will act to prevent the naturally collapsed GI tract wall from penetrating the capsule's leg cavity.

The advantage of the vertical configuration of the micromotor is that it allows for a very compact design (270 mm^3) resulting in the most efficient use of space. The two legs, central support, leg ties, and the microrobot case will absorb the load from the GI tract wall. The compact gearing allows the rate at which the legs are deployed to be controlled by the ratio of the gear train.

A. Gear Train

For the holding mechanism to operate at a safe speed, the micromotor will require the gear train to slow it down. The chosen micromotor is manufactured by Faulhaber and already has an integral gearbox, which reduces the 20 000 r/min by a factor of 13:1. This results in a starting RPM of 1538 r/min, which is significantly high; therefore, further reductions will be

TABLE II
ESTIMATED GEAR TRAIN OUTPUT FROM AN INPUT OF 1538 R/MIN

Gear stages	Micromotor and bevel gear	Bevel gear and spur gear	Second stage spur gear	Output spur gear
No. of teeth on driver (d)	13	8	8	8
No. of teeth on follower (f)	48	34	34	22
Output RPM	417.93	98.34	23.14	8.41

achieved from the gear train. The output speed of a gear train can be estimated from the following equation:

$$\text{RPM}_{\text{out}} = \frac{N_{d1} \times N_{d2} \times N_{d3} \times N_{d4} \times \text{RPM}_{\text{in}}}{N_{f1} \times N_{f2} \times N_{f3} \times N_{f4}} \quad (1)$$

where RPM_{in} is the input speed, N_{d1} is the number of teeth on the driving gear, and N_{f1} is the number of teeth on the follower gear. This formula can be applied to the gear train with a selection of gear teeth to determine the output RPM; see Table II.

As can be seen from Table II, the number of teeth on the follower gears is higher than the number of teeth on the driving gears; this is to ensure a rapid reduction in RPM in the minimum amount of space. The target is to deploy the holding mechanism as slowly as possible as this will reduce the potential for trauma to the GI tract wall from the legs and supports. However, there are limitations to the number of teeth which can be used as the chosen gear module, which is the ratio of the pitch diameter to the number of teeth on the gear, and which determines the overall geometry of the gear. The chosen bevel gear module is 0.2; this results in a maximum number of teeth of 48 and an overall gear diameter of 10.0 mm [see Fig. 4(a)] as the gear has the overall limiting factor of the diameter of the microrobot. The spur gears use a module of 0.1; this results in a maximum number of teeth of 34 as the gears are required to be linked together in a train [see Fig. 4(b)]; they are, therefore, limited again to the overall diameter of the microrobot.

The gear train results in a reduction of 1538 to 8.4 r/min. This reduced output speed will deploy the legs in approximately 1.8 s; altering the number of teeth on the driver or follower will increase or decrease this figure.

An important function of the gear train is to transmit power from the micromotor to the legs; this will enable the legs to distend the luminal wall and hold the microrobot in position. The power transmitting capacity of a gear train can be determined by the following formula:

$$T_{\text{out}} = \frac{N_{f1} \times N_{f2} \times N_{f3} \times N_{f4} \times T_{\text{in}}}{N_{d1} \times N_{d2} \times N_{d3} \times N_{d4}} \quad (2)$$

where T_{in} is the input torque, N_{f1} is the number of teeth on the follower gear, and N_{d1} is the number of teeth on the driving gear. Applying this formula to the gear train and using 0.15 mN·m torque generated by the Faulhaber micromotor as the input torque T_{in} results in an estimated output torque T_{out} of 27.5 mN·m.

B. Analysis of Holding Mechanism Arms

To attain a state of equilibrium, the external forces acting on the microrobot must be balanced for any given orientation; however, angles less than 90° from the horizontal can be neglected from the equilibrium analysis, as in the worst case the load would be acting vertical to the horizontal resulting in a multiplication factor of $\sin 90$ which equals 1, hence producing no net increase in load. Fig. 5 shows the external forces acting on the legs of the microrobot. For the force analysis, the contact area has been divided into six contact points as these points will be in continuous contact with the GI tract wall throughout the deployment of the mechanism.

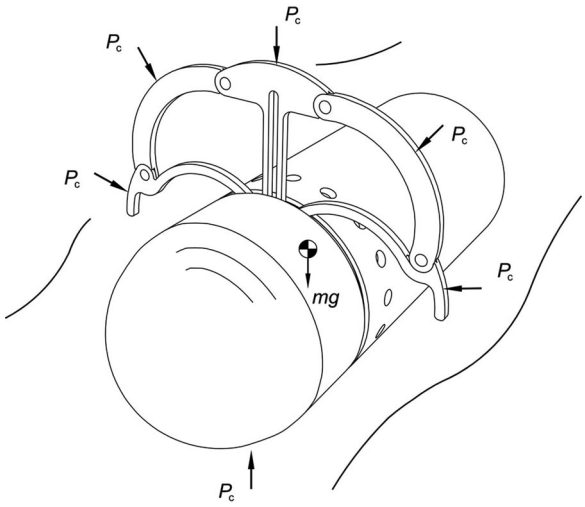

Fig. 5. External radial peristaltic force P_c acting on the microrobot at six positions.

As can be seen from Fig. 5, the external forces acting on the microrobot's legs are the circumferential peristaltic force P_c; the linear peristaltic forces are neglected as they do not contribute to the holding function and through FEA analysis it has been shown that they are not sufficiently strong to cause any deformation of the mechanism. Using the figures determined by Miftahof [11], the circumferential amplitude of 26.9 g/cm results in an estimated load of 720.8 mN for the total circumferential contact area of the extended legs and microrobot's body.

The micromotor employed to drive the legs must be capable of delivering an equivalent force to the legs to maintain a state of equilibrium. The force acting at each point of contact P_c can be estimated by the following formula:

$$P_c = \frac{F_c + mg}{6} \quad (3)$$

where F_c is the circumferential force from the GI tract wall and mg is the weight of the microrobot.

The load acting at each point equates to 120.1 mN; however, this load will work toward preventing the legs from opening.

C. Load Points P_c Contributing to Torque

The process of operating the legs from the stored position to the fully extended position results in the circumferential force from the GI tract wall P_c acting toward the center of the microrobot. However, only the perpendicular component force F_{p1} will be working to prevent the legs from opening. This is illustrated for leg 1 in Fig. 6.

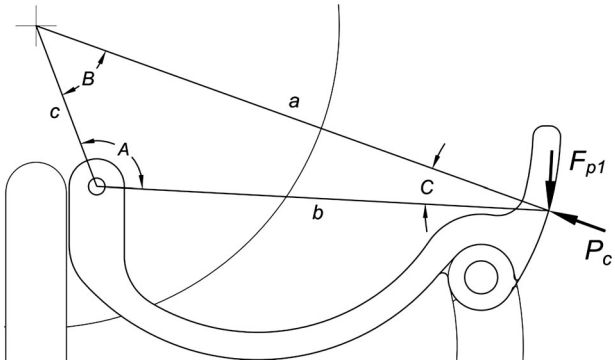

Fig. 6. Component force F_{p1} of the radial peristaltic force P_c acting on the microrobot's leg.

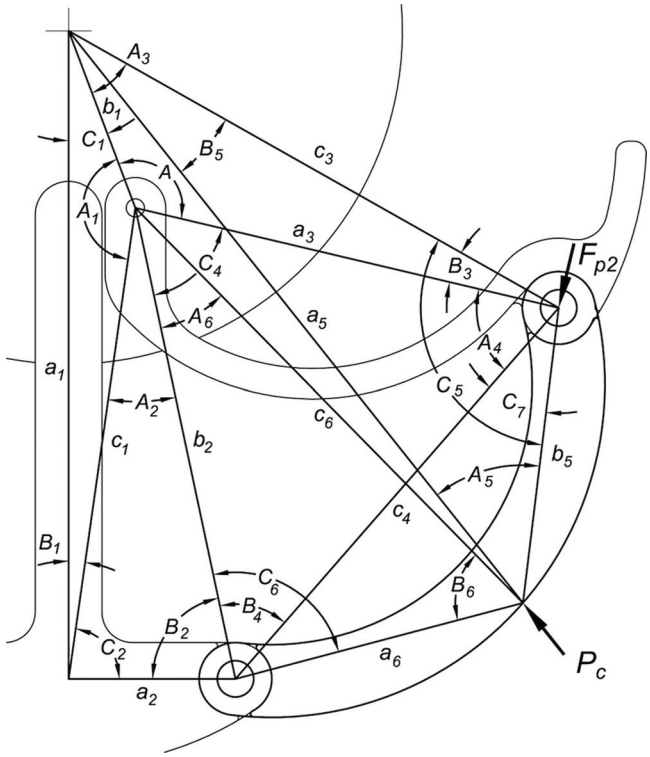

Fig. 7. Component force F_{p2} of the radial peristaltic force P_c acting on the microrobot's tie bar. The tie bar links the leg to the center support.

The perpendicular component force F_{p1} (see Fig. 6) can be estimated for a leg movement through zero° to 90° using the following formula:

$$F_{p1} = P_c \left(\frac{c(\sin A)}{\sqrt{b^2 + c^2 - 2bc(\cos A)}} \right). \tag{4}$$

The perpendicular component force F_{p2} acting on tie bar 1 can be seen in Fig. 7 and can be estimated as follows:

$$F_{p2} = P_c \cos\left[\tan^{-1}\left(c_3\left(\frac{\sin C_5}{b_5 - (c_3 \cos C_5)}\right)\right)\right] \sin\left[\cos^{-1}\left(\left({a_3}^2 + {b_2}^2 + {c_4}^2\right) - \left(\frac{{b_2}^2}{2a_3 c_4}\right)\right) + C_7\right]. \tag{5}$$

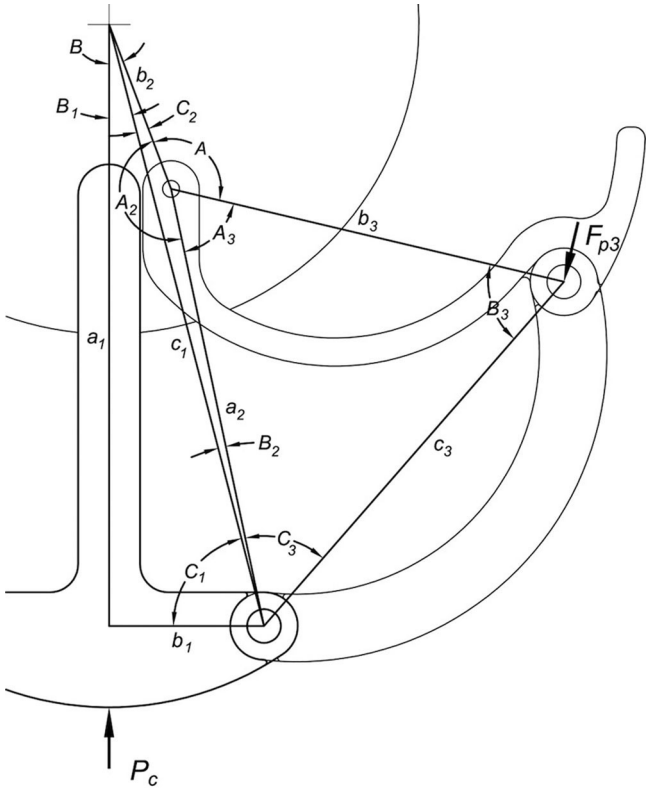

Fig. 8. Component force F_{p3} of the radial peristaltic force P_c acting on the microrobot's center support.

The radial peristaltic force P_c acting on the center support (see Fig. 8) would be split between the two pivot points linking the two tie bars; however, the sum of the two points would count toward the torque requirement. As the geometry and loading are symmetrical, only one side of the center support requires analysis; this can be seen in Fig. 8 and can be estimated as follows:

$$F_{p3} = \left[\frac{P_c}{\sin(180 - (C_3 + B_2 + C_1))}\right] \sin\left[\tan^{-1}\left(\frac{a_2 \sin A_3}{b_3 - (b_2 \cos A_3)}\right)\right]. \tag{6}$$

Equation (6) uses the total peristaltic force P_c; therefore, the resulting component force F_{p3} represents the total component force from both pivot points of the center support.

The three individual perpendicular component forces F_{p1}, F_{p2}, and F_{p3} can be combined with F_{p4} the perpendicular component forces for tie bar 2 and F_{p5} the perpendicular component forces acting on leg 2 to find the maximum load which will be delivered to the micromotor through the zero° to 90° leg movement. Fig. 9 shows a plot of the individual loads through the full movement and the resulting combined load F_p.

The result of the combined plots (see Fig. 9) shows the maximum load of 378.15 mN acting on the final gear in the gear train to be at 90°; this results in a torque of 2.78 mN·m acting on the gear. However, the estimated results of (2) show an output torque T_{out} for the gear train to be 27.5 mN·m; this gives a high margin of safety before the micromotor stalls. The holding

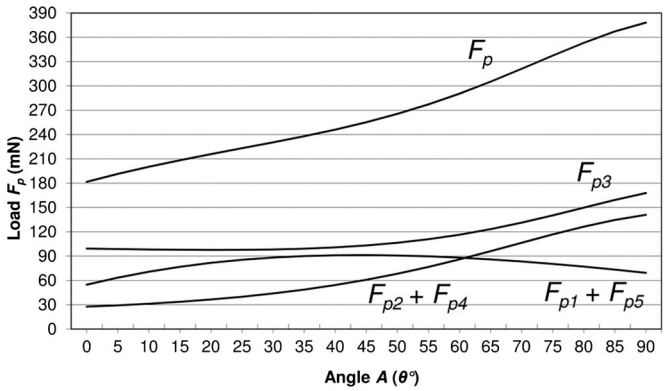

Fig. 9. Graph showing the individual perpendicular component forces $F_{p1}, F_{p2}, F_{p3}, F_{p4}$, and F_{p5} generated by the GI tract acting on the holding mechanism and the total combined load F_p, which will act to prevent the holding mechanism from operating.

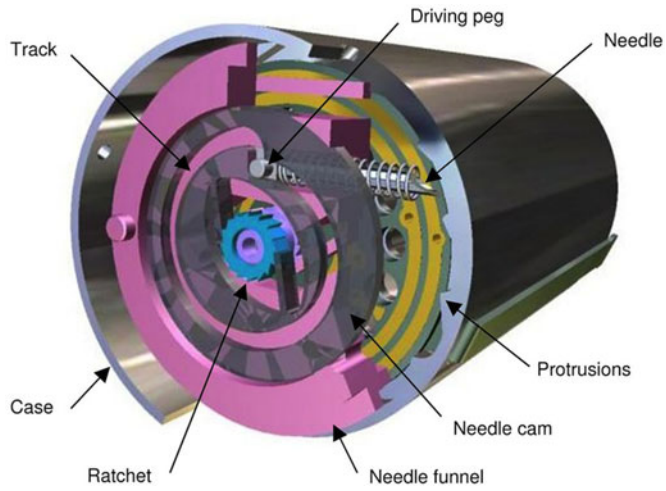

Fig. 10. Needle positioning mechanism assembly with material removed for clarity. Needle shown in the fully retracted position.

mechanism has been designed to withstand the estimated force the GI tract wall can generate. A system validation including *in vivo* measurements is required to verify these results.

The 6-point loads have been used to confirm the stability of the mechanism through FEA analysis. Using the FEA process, the thickness of the arms was optimized; however, the areas that contact the GI tract wall may be increased in future trials to limit any potential trauma to the GI tract wall.

IV. Targeting and Drug Delivery Mechanism

A. Needle Positioning Mechanism

A single micromotor orientated along the axis of the microrobot's body is used to drive the needle positioning mechanism (see Fig. 10). The needle positioning mechanism utilizes a 1.5-mm diameter × 10.5-mm-long micromotor manufactured by Namiki, a needle funnel, a movable needle, a needle cam, and two opposing ratchets. Also, features integral to the microrobot's body are required (protrusions). The sequence of operation is to first position the needle angularly followed by the extension of the needle and delivery of the medication; then the needle is retracted. The supply of medication will be stored in a sealed section of the body and be delivered through the needle by means of a piston. Rapid delivery of the medication will be achieved through the activation of a conical shape memory alloy (SMA) compression spring. Activating the spring by means of the Joules effect will remove the need for a bulky complex trigger system to release the spring.

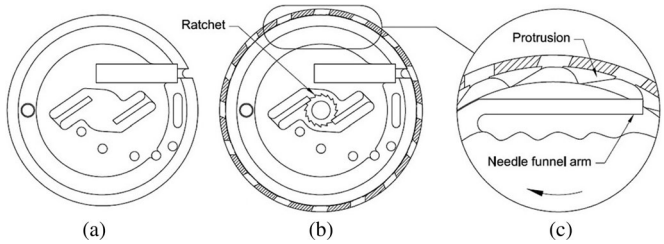

Fig. 11. Needle positioning mechanism: (a) needle funnel, (b) ratchet driving the needle funnel, which has material removed, and (c) needle funnel arm engaged with a protrusion.

The needle positioning mechanism is capable of positioning the needle at a number of points in a 360° envelope; however, for the purpose of prototyping 16 fixed positions equally spaced have been chosen. The angular positioning of the needle is achieved by the anticlockwise rotation of the micromotor while the advancement and retraction of the needle is achieved by the clockwise rotation of the micromotor.

B. Positioning the Needle

Maneuvring the needle to a selected position is achieved by applying a negative voltage to the micromotor. The negative voltage will cause the micromotor to rotate in an anticlockwise direction. The needle funnel as shown in Fig. 11(a) rotates anticlockwise by virtue of a ratchet, which is mounted on the micromotor's driveshaft. The ratchet engages with a set of sprung legs which are integral to the needle funnel [see Fig. 11(b)] . The needle is engaged with the needle funnel and is carried round with it.

When the needle funnel is rotating anticlockwise, an arm which protrudes from the side of the needle funnel rides over the top of a plurality of protrusions [see Fig. 11(c)] on the inside face of the body. The function of these protrusions is to prevent the needle funnel from rotating clockwise when the motor is reversed. It achieves this by engaging the end of the arms with a parallel surface of the protrusion [see Fig. 11(c)] preventing any further movement clockwise and aligning the needle with one of the 16 fixed ports on the microrobot's body.

C. Operating the Needle

Applying a positive voltage to the micromotor reverses its direction, this disengages the needle funnel ratchet from its sprung legs and engages the needle cam ratchet with a set of sprung legs that are integral to the needle cam (see Fig. 12).

When engaged, the ratchet drives the needle cam in a clockwise direction. The needle is engaged with a track in the needle cam by means of a driving peg mounted on the side of the needle (see Fig. 12). The track is shaped to convert the rotational

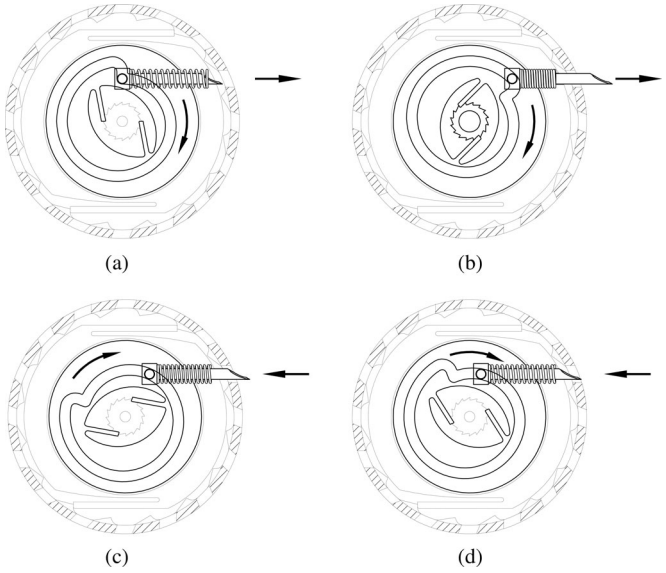

Fig. 12. 360° needle cam operating cycle: (a) stored position, (b) full stroke, (c) needle returning to the stored position, and (d) retracted position.

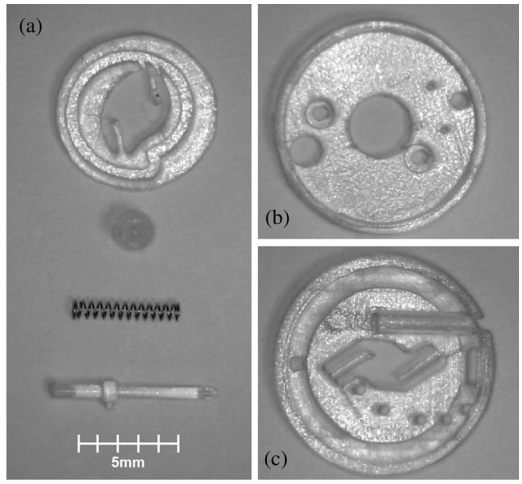

Fig. 13. 1:1 scale SLA prototypes: (a) needle cam, ratchet, spring, and needle combined with the driving peg, (b) retaining cover, and (c) needle funnel.

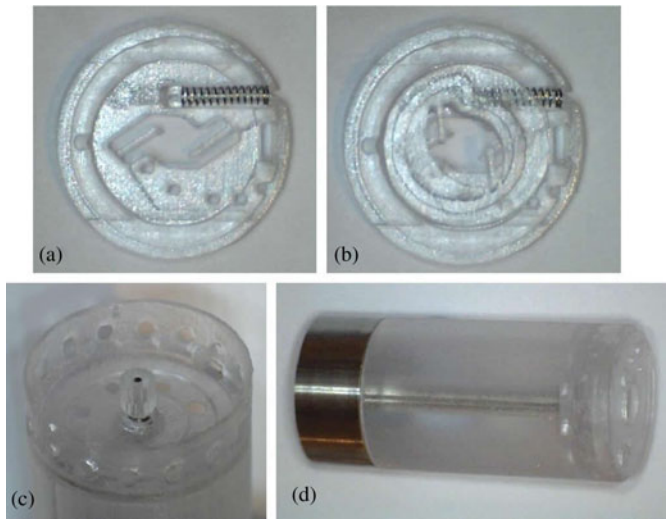

Fig. 14. Assembled needle positioning mechanism: (a) needle funnel, spring, and needle assembled, (b) needle cam in position, (c) ratchet and case cavity, and (d) case fitted with the mechanism and coupled to a drive spindle.

motion of the cam into a variable linear motion. This linear motion allows the advancement and retraction of the needle.

Fig. 12 shows the sequence of operation for the extension and retraction of the needle. Fig. 12(a) shows the needle in the stored position; this is the position the needle will be in when the microrobot is swallowed and travels through the GI tract to the target site. A compression spring is used to ensure that the driving peg maintains contact with the track and also that the needle returns to the start position. Fig. 12(b) shows the needle at full extension giving a reach of approximately 6.9-mm radius and a stroke length of 2.0 mm. The design of the cam utilizes a direct linear movement so that a positive force can be delivered to the needle that will be required to penetrate the wall of the GI tract. Fig. 12(c) shows the needle retracting by virtue of the track slowly spiralling inward and the pressure exerted by the spring. Fig. 12(d) shows the needle returning to the stored position once the medication has been delivered. Further, design analysis of the targeting mechanism has been described in detail in the previous work [17].

Fig. 13 shows the component parts of the needle positioning mechanism. All the parts except the stainless steel spring have been prototyped using a high-resolution stereolithography (SLA) manufacturing process. The one-to-one scaled prototypes are manufactured from Accura 60, which is a resin with similar mechanical properties to polycarbonate.

The assembled needle positioning components can be seen in Fig. 14. Fig. 14(a) shows the needle funnel fitted with the needle and spring. Fig. 14(b) shows the needle cam mounted in the needle funnel and engaged with the needle's drive peg. Fig. 14(c) shows the ratchet mounted on a drive spindle, and the cavity in the case which will house the targeting mechanism. Fig. 14(d) shows the case fitted with the mechanism and the drive spindle at the rear.

The proof-of-concept prototypes perform within the allowable design limits with all the arms flexing and returning to their original positions. The spring allows the needle to advance 2.0 mm and then return back to rest.

V. Additional Platform Considerations

In order to complete a system realization of a targeted drug delivery platform, there are several aspects which, although outside the scope of this paper, are necessary to realize. This section will detail these considerations.

A. Localization

It is an important requirement that the location of the microrobot is known when it passes through the GI tract [18]. The spatial information will be used to determine where potential pathologies have been located, and hence give the ability to return to these sites for follow-up treatment.

One method reported in the literature for following the progress of a WCE through the GI tract is through the

monitoring of the magnetic field strength of an on-board permanent magnet [19]. Using a magnetic tracking algorithm and a magnetoresistive sensor array attached to the skin, the position and orientation of the microrobot can be estimated. Figures reported by Wang *et al*. [20] show average position errors of 3.3 mm and average orientation errors of 3°; however, the number of external sensors will determine the overall accuracy of the system.

A widely used approach to localization is through the monitoring of electromagnetic waves [19]. Radio frequency triangulation is employed on the M2A by Given Imaging. This method utilizes the received signal strength of the images which are being transmitted to eight external receivers to determine the position of the device. The average position error of this method is 37.7 mm; however, this method is limited to 2-D positioning [21].

There are alternative methods to localization such as gamma scintigraphy. This method is employed on the InteliSite [7] by Innovative Devices LLC. The capsule can be tracked through the GI tract using gamma scintigraphy, which will detect Indium (111In) or Technetium (99mTc) gamma isotopes that have been incorporated into the capsule. However, the locational accuracy of the system is limited as capsule orientation cannot be determined, and only the capsule's general position within the GI tract can be ascertained.

It is intended that additional monitoring methods such as recording pH levels and transit time will be combined with a localization method to give an overall indication of the capsule's location.

B. Electronics

It is crucially important to consider the various components and wiring in such a space-constrained design. Key electronic components include the following.

1) CMOS Image Sensor: This design uses a commercially available subminiature image sensor manufactured by Toshiba (TCM8230MDA) with four white SMT LEDs manufactured by Agilent (HSMW-C191) integrated on a PCB.

2) Rotary Encoder and Wiring: The microrobot can be split into four sections: the visualization and processing section, the needle positioning mechanism, the holding mechanism, and the power supply section. Fig. 15 highlights these sections with a cut-through view of the microrobot.

The configuration of the four sections of the microrobot presents problems of power delivery, specifically delivering power to the holding mechanism, and the visualization and processing section. This is due to the requirement that the holding mechanism can be deployed diametrically opposite the needle, as this requires the front section of the microrobot to be able to rotate 360°.

The solution is to run power lines on the outside of the body from the power supply to a rotary encoder board; this bypasses the need to disrupt the medication compartment. The rotary encoder board has four concentric tracks equally spaced. Contact pins held in the needle positioning mechanism can contact the tracks yet still remain free to rotate. A fifth contact pin is used in conjunction with a registration contact on the rotary encoder board to determine the angular position of the needle and holding mechanism.

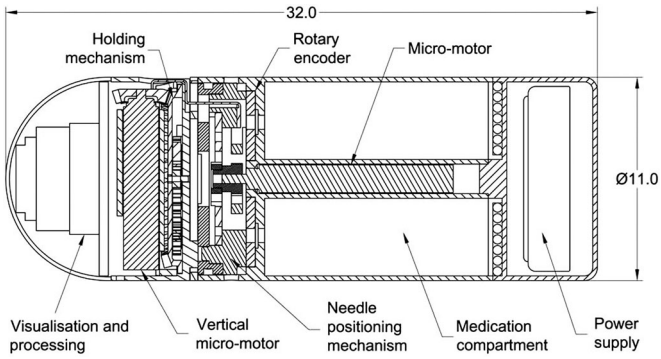

Fig. 15. Cut-through view of the microrobot with the four main sections labeled.

3) Controller ASIC: The power management (i.e., dc/dc conversion), telemetry, timing, and control are being implemented in a full-custom ASIC in a commercially available 0.18-μm CMOS technology. Much of the specific circuit implementations will be based on previously reported systems [22]–[24].

C. Energy Requirements

As the space available for the power supply onboard the WCE is limited, it is essential that the needle positioning mechanism and the holding mechanism can both operate with low power consumption. The energy requirements for both mechanisms have been estimated from the peak current consumption of the Namiki motor controller (SSD04) and the Faulhaber motor controller (BLD05002S), which are stated as 800 mA at 6 V and 400 mA at 7.5 V. Three revolutions of the Namiki micromotor are required for positioning and deployment of the needle; this is achieved in 3.8 s while the holding mechanism can complete a full opening and closing cycle in 1.78 s. Using a Lithium coin battery with a volume of 188 mm^3 and an energy density of 435 Wh/L (CR1025 Energizer), the mechanisms will consume at most 28.94 J of energy for each complete cycle which is only 9.8% of the available energy, offering the potential for multiple operations.

VI. Conclusion

In this paper, the authors have presented a novel targeted drug delivery platform toward the realization of a practical micropositioning system and holding mechanism for targeted drug delivery in the small intestines. The platform can be used for the detection and treatment of pathologies of the GI tract such as Crohn's disease, small intestinal tumors such as lymphoma and small intestinal cancer.

It has been shown that the proposed needle positioning mechanism and the holding mechanism achieve the required functionality while occupying a combined volume of less than 470 mm^3. This is based on the proposed needle positioning mechanism and

holding mechanism consuming a maximum of 28.94 J of energy per operation.

The targeted drug delivery platform has the control necessary to target a particular pathogen within the GI tract. It is envisaged that a delivery mechanism capable of delivering 1 ml of medication to the target site can be incorporated into the standard geometry of the WCE, with the combined needle positioning system, holding mechanism, and delivery mechanism (including 1 ml of medication) occupying 60% of the total available volume.

The research so far has been focused on the analysis of the novel micropositioning mechanism and the holding mechanism. During *in vitro* testing and validation, these systems will be tested to determine if the needle positioning mechanism has sufficient power to penetrate the GI tract wall and that the holding mechanism has sufficient power to overcome peristalsis. An area for consideration is the miniaturization of the electronics and the development of a control system with a user interface.

ACKNOWLEDGMENT

The authors would like to thank Consultant Physician N. Oliver for clinical insight and much useful discussion and P. Pendergast, Head of Prototyping and Production, at IDC Models Ltd. for his invaluable help in producing the prototypes.

REFERENCES

[1] G. D. Meron, "The development of the swallowable video capsule (M2A)," *Gastrointest. Endosc.*, vol. 52, pp. 817–819, 2000.

[2] P. Swain and A. Fritscher-Ravens, "Role of video endoscopy in managing small bowel disease," *Gut*, vol. 53, no. 12, pp. 1866–1875, 2004.

[3] D. R. Cave, D. E. Fleischer, J. A. Leighton, D. O. Faigel, R. I. Heigh, V. K. Sharma, C. J. Gostout, E. Rajan, K. Mergener, A. Foley, M. Lee, and K. Bhattacharya, "A multicenter randomized comparison of the endocapsule and the pillcam SB," *Gastrointest. Endosc.*, vol. 68, pp. 487–494, 2008.

[4] J. L. Toennies, G. Tortora, M. Simi, P. Valdastri, and R. J. Webster III, "Swallowable medical devices for diagnosis and surgery: The state of the art," *J. Mechan. Eng. Sci.*, vol. 224, pp. 1397–1414, 2010.

[5] N. I. Goldfarb, L. T. Pizzi, J. P. Fuhr, C. Salvador, V. Sikirica, A. Kornbluth, and B. Lewis, "Diagnosing crohn's disease: An economic analysis comparing wireless capsule endoscopy with traditional diagnostic procedures," *Disease Manag.*, vol. 7, pp. 292–304, 2004.

[6] A. Forgione, "*In vivo* microrobots for natural orifice transluminal surgery. current status and future perspectives," *Surg. Oncol.*, vol. 18, pp. 121–129, 2009.

[7] I. Wilding, P. Hirst, and A. Connor, "Development of a new engineering-based capsule for human drug absorption studies," *Pharma. Sci. Technol. Today*, vol. 3, pp. 385–392, 2000.

[8] P. J. Houzego, P. N. Morgan, P. H. Hirst, D. J. Westland, and I. R. Wilding, "Ingestible device for the release of substances at distinct locations in the alimentary canal," U.S. Patent US 006 884 239 B2, 2005.

[9] H. Gray, *Gray's Anatomy*. London: Greenwich Editions, 2005.

[10] W. Xiaona, M. Q. H. Meng, and C. Yawen, "Physiological factors of the small intestine in design of active capsule endoscopy," in *Proc. Annu. Int. Conf. IEEE Eng. Med. Biol. Soc.*, Jan. 2005, pp. 2942–2945.

[11] R. N. Miftahof, "The wave phenomena in smooth muscle syncytia," *Silico Biol.*, vol. 5, pp. 479–498, 2005.

[12] H. Park, S. Park, E. Yoon, B. Kim, J. Park, and S. Park, "Paddling based microrobot for capsule endoscopes," in *Proc. IEEE Int. Conf. Robot. Autom.*, Apr. 2007, pp. 3377–3382.

[13] S. H. Woo, T. W. Kim, and J. H. Cho, "Stopping mechanism for capsule endoscope using electrical stimulus," *Med. Biol. Eng. Comput.*, vol. 48, pp. 97–102, 2010.

[14] F. Carpi, S. Galbiati, and A. Carpi, "Controlled navigation of endoscopic capsules: Concept and preliminary experimental investigations," *IEEE Trans. Biomed. Eng.*, vol. 54, no. 11, pp. 2028–2036, Nov. 2007.

[15] P. Valdastri, R. J. Webster, C. Quaglia, M. Quirini, A. Menciassi, and P. Dario, "A new mechanism for mesoscale legged locomotion in compliant tubular environments," *IEEE Trans. Robot.*, vol. 25, no. 5, pp. 1047–1057, Oct. 2009.

[16] A. Connor, P. Evans, J. Doto, C. Ellis, and D. E. Martin, "An oral human drug absorption study to assess the impact of site of delivery on the bioavailability of bevirimat," *J. Clin. Pharmacol.*, vol. 49, pp. 606–612, 2009.

[17] S. P. Woods and T. G. Constandinou, "Towards a micropositioning system for targeted drug delivery in wireless capsule endoscopy," in *Proc. Annu. Int. Conf. IEEE Eng. Med. Biol. Soc.*, Aug./Sep. 2011, pp. 7372–7375.

[18] G. Ciuti, A. Menciassi, and P. Dario, "Capsule endoscopy: From current achievements to open challenges," *IEEE Rev. Biomed. Eng.*, vol. 4, pp. 59–72, 2011.

[19] T. D. Than, G. Alici, H. Zhou, and W. Li, "A review of localization systems for robotic endoscopic capsules," *IEEE Trans. Biomed. Eng.*, vol. 59, no. 9, pp. 2387–2399, Sep. 2012.

[20] X. Wang, M.-H. Meng, and C. Hu, "A localization method using 3-axis magnetoresistive sensors for tracking of capsule endoscope," in *Proc. Annu. Int. Conf. IEEE Eng. Med. Biol. Soc.*, Aug./Sep. 2006, pp. 2522–2525.

[21] D. Fischer, R. Schreiber, D. Levi, and R. Eliakim, "Capsule endoscopy: The localization system," *Gastrointest. Endosc. Clin. North Amer.*, vol. 14, pp. 25–31, 2004.

[22] X. Xie, G. Li, X. Chen, X. Li, and Z. Wang, "A low-power digital ic design inside the wireless endoscopic capsule," *IEEE J. Solid-State Circuits*, vol. 41, no. 11, pp. 2390–2400, Nov. 2006.

[23] B. Chi, J. Yao, S. Han, X. Xie, G. Li, and Z. Wang, "Low-power transceiver analog front-end circuits for bidirectional high data rate wireless telemetry in medical endoscopy applications," *IEEE Trans. Biomed. Eng.*, vol. 54, no. 7, pp. 1291–1299, Jul. 2007.

[24] X. Chen, X. Zhang, L. Zhang, X. Li, N. Qi, H. Jiang, and Z. Wang, "A wireless capsule endoscope system with low-power controlling and processing ASIC," *IEEE Trans. Biomed. Circuits Syst.*, vol. 3, no. 1, pp. 11–22, Feb. 2009.